

Forschungszentrum Karlsruhe

Technik und Umwelt

Wissenschaftliche Berichte

FZKA 6672

Mixed Convection in a Two-Phase Flow Cooling Loop

G. Janssens-Maenhout, M. Daubner, J. U. Knebel

Institut für Kern- und Energietechnik
Programm Nukleare Sicherheitsforschung

Forschungszentrum Karlsruhe GmbH, Karlsruhe
2002

Impressum der Print-Ausgabe:

**Als Manuskript gedruckt
Für diesen Bericht behalten wir uns alle Rechte vor**

**Forschungszentrum Karlsruhe GmbH
Postfach 3640, 76021 Karlsruhe**

**Mitglied der Hermann von Helmholtz-Gemeinschaft
Deutscher Forschungszentren (HGF)**

ISSN 0947-8620

Abstract

One possible concept for the passive decay heat removal from the containment of an innovative, future light water reactor after a core melt accident is based on passive sump cooling. In such a concept the core-melt would be spread and stabilised on the initially dry reactor sump area. After a number of plugs on flooding pipes melt through by passive means, water from the in-containment refueling water storage tanks (IRWST) would flood the core melt with a low flow rate from above. The sump cooling is achieved by a stable natural circulation flow which transports the decay heat from the core melt to condensers and heat exchangers located within the sump area. The passive heat transfer mechanisms within the containment are vapourisation/condensation, convection and conduction. The experimental and numerical work on the Sump COoling programme SUCO allowed to obtain results on the feasibility of the concept and on stable points of operation.

The SUCO Programme at Forschungszentrum Karlsruhe was performed within the POOLTHY Project of the Euratom Fourth Framework Programme (FP) on evolutionary reactor safety concepts.

This report summarizes the numerical simulations using the CFD code CFX4.1 which has additional models for subcooled flow boiling phenomena and the interfacial forces. The improved CFX4.1 code can be applied to the design of boiling induced mixed convection cooling loops in a defined parameter range. The experimental part describes the geysering experiments and the instability effects on the two-phase natural circulation flow. An experimentally validated flow pattern map in the Phase Change Number - Subcooling Number ($N_{PCh} - N_{Sub}$) diagram defines the operational range in which flow instabilities such as geysering can be expected.

One important perspective of this combined experimental/numerical work, which is in the field of two-phase flow, is its application to the development of accelerator driven systems (ADS). The main objective on an ADS is its potential to transmute minor actinides and long-lived fission products, thus participating in closing the fuel cycle. The development of an ADS is an important issue within the Euratom Fifth FP on Partitioning and Transmutation.

One concept of an ADS, which is investigated in more detail within the "Preliminary Design Study of an eXperimental ADS" Project (PDS-XADS) of the Euratom Fifth FP, is the XADS lead-bismuth cooled Experimental ADS of ANSALDO. An essential feature of this concept is the natural circulation of the primary coolant within the reactor pool. The natural circulation, which is driven by the density differences between the blanket and the heat exchanger, is enhanced by the injection of the nitrogen cover gas through spargers located in a riser part just above the blanket.

This so-called gas-lift pump system has not been investigated in more detail nor has this gas-lift pump system been numerically/experimentally confirmed.

The knowledge gained within the SUCO Programme, i. e. the modelling of the interfacial forces, the experimental work on flow instabilities and the modelling of the interfacial area concentration, can be directly applied to the design of accelerator driven systems (ADS). However, the transfer from the two-phase system water / steam to the system lead-bismuth / nitrogen still has to be done.

Thus, the results of the POOLTHY Project are partly of direct relevance to the Programme on Partitioning and Transmutation and especially to the PDS-XADS Project.

Mischkonvektionsströmung eines zweiphasigen Kühlkreislaufs

Zusammenfassung

Ein mögliches Konzept für die passive Nachwärmeabfuhr aus dem Sicherheitsbehälter eines innovativen Leichtwasserreaktors nach einem Kernschmelzunfall ist das Sumpfkühlkonzept. In diesem Konzept würde die Kernschmelze in dem anfänglich trockenen Reaktorsumpf ausgebreitet und stabilisiert werden. Nach dem passiven Durchschmelzen von Kappen auf Flutrohren würde Wasser aus dem anlageninternen Flutwasser-Vorratsbehälter (IRWST) die Kernschmelze unter einem geringen Volumenstrom von oben fluten. Die Kühlung wird durch die Ausbildung einer stabilen Naturkonvektionsströmung im Sumpf erreicht, die die Wärme von der Kernschmelze an Kondensatoren und Wärmetauscher transportiert, die im Sumpfbereich angeordnet sind. Die passiven Mechanismen der Wärmeübertragung sind Verdampfung/Kondensation, Konvektion und Wärmeleitung. Die experimentellen und numerischen Arbeiten des Sumpfkühl-Programms SUCO erlauben Aussagen zur Machbarkeit des Sumpfkühlkonzepts und zu stabilen Betriebspunkten.

Das SUCO Programm am Forschungszentrum Karlsruhe wurde innerhalb des POOLTHY Projekts des Euratom Fourth Framework Programme (FP) zu evolutionären Reaktorsicherheitskonzepten durchgeführt.

Dieser Bericht fasst die numerischen Simulationsrechnungen mit dem Rechenprogramm CFX4.1 zusammen, welches um Modelle zum unterkühlten Strömungssieden und zu den Zwischenphasenkräften erweitert ist. Das verbesserte CFX4.1 Programm kann zum Entwurf von Kühlkreisläufen unter Mischkonvektion, die durch Siedephänomene angetrieben sind, in einem definierten Parameterbereich herangezogen werden. Der experimentelle Teil beschreibt die Versuche zum Geysering und zu Instabilitätseffekten, die bei einer zweiphasigen Naturkonvektionsströmung auftreten können. Die ausgemessene Strömungskarte, die die Phasenübergangs-Zahl (N_{PCh}) als Funktion der Unterkühlungs-Zahl (N_{Sub}) darstellt, definiert den Anwendungsbereich, in dem Strömungsinstabilitäten wie zum Beispiel Geysering zu erwarten sind.

Eine wichtige Perspektive dieser experimentellen und numerischen Arbeit im Bereich der Zweiphasenströmung ist ihre Anwendbarkeit für die Entwicklung eines Beschleuniger getriebenen Systems (ADS). Die wesentliche Zielsetzung eines ADS ist die Transmutation von Minoren Aktiniden und langlebigen Spaltprodukten und somit die Schließung des Brennstoffkreislaufs. Die Entwicklung eines ADS ist ein wichtiger Schwerpunkt im Euratom Fifth FP zur Wiederaufarbeitung und Transmutation.

Ein Konzept eines ADS, das intensiver im Projekt "Preliminary Design Study of an eXperimental ADS" (PDS-XADS) des Euratom Fifth FP untersucht wird, ist der Experimental ADS von ANSALDO, der Blei-Wismut als Kühlmittel verwendet. Ein wesentliches Merkmal dieses Konzepts ist die Naturkonvektionsströmung des Primärkühlmittels im Reaktortank. Die Naturkonvektionsströmung, die von dem Dichteunterschied zwischen Kern und Wärmetauscher angetrieben wird, wird durch das Einperlen von Stickstoff durch Düsen, die oberhalb des Kerns angeordnet sind, verstärkt.

Dieses sogenannte Gashub-Pumpensystem ist noch nicht im Detail untersucht worden, es ist weder numerisch noch experimentell untermauert worden.

Das im Rahmen des SUCO Programms gewonnene Wissen, d. h. die Modellierung der Zwischenphasenkräfte, die experimentellen Arbeiten zu Strömungsinstabilitäten und die Modellierung der Zweiphasengrenzflächen-Konzentration, kann direkt für die Entwicklung eines Beschleuniger getriebenen Systems (ADS) eingesetzt werden. Allerdings muss die Übertragung des Zweiphasensystems Wasser/Wasserdampf auf das System Blei-Wismut/Stickstoff noch geleistet werden.

Somit sind die Ergebnisse des POOLTHY Projekts teilweise von direkter Bedeutung für das Programm zu Wiederaufarbeitung und Transmutation, besonders für das Projekt PDS-XADS.

Contents

1	Introduction.	7
1.1	Nuclear Safety Background.	7
1.2	Sump Cooling Concept.	7
1.3	Objective.	9
2	Experimental Setup.	11
2.1	Description.	11
2.2	Equipment and Instrumentation.	12
2.3	Scaling.	13
2.4	Experimental Conditions.	14
2.5	Operating Range and Stability Limits.	15
3	Numerical Simulation.	17
3.1	Model Assumptions and Equations.	17
3.2	Boundary Conditions and Initial Flow.	18
3.3	Subcooled Boiling in the Horizontal Duct.	19
3.3.1	Bubble Formation.	20
3.3.2	Bubble Detachment.	20
3.3.3	Heat Balance at the Wall.	20
3.3.4	Condensation in the Subcooled Bulk.	20
3.4	Bubbly Flow in the Chimney.	21
3.5	Concluding Numerical Results.	23
4	Geysering Experiments.	25
4.1	Description of the Phenomena.	25
4.2	Instability Properties of the Test Facility.	27
4.3	Characteristic Pressure Behaviour.	28
4.4	Characteristic Profile of the Geysering Strength.	28
4.4.1	Geysering Strength as Function of the Wall Heat Flux.	28
4.5	Characteristic Profile of the Geysering Frequency.	29
4.5.1	Geysering Frequency as Function of the Wall Heat Flux	29
4.5.2	Geysering Frequency as Function of the Initial Hydrostatic Head.	30
4.5.3	Geysering Frequency as Function of the Riser Width.	31
4.6	Concluding Experimental Results.	32
5	Conclusion.	33

6 Perspectives	35
Bibliography	37
Acknowledgement	37
7 Appendix 1: Prototype Conditions.	43
8 Appendix 2: List of Symbols	45

Chapter 1

Introduction.

1.1 Nuclear Safety Background.

Although modern nuclear power plants reach a very high safety and availability level, innovative modifications improving the capacity and reliability are under consideration, Kuczera et al. (1994). Nowadays mainly simple systems with passive components are pursued because of their reliable and cheap operation without human intervention. In this report a passive sump cooling concept from Weißhäupl and Bittermann (1993) is investigated in more detail, which considers a spreading of the core melt on a large area, its flooding with sump water and its cooling by a passive two-phase/single-phase natural circulation flow within the sump volume. Such natural circulation loops and boiling induced convection loops are strongly envisaged in emergency core cooling systems for advanced pressurised water reactors or in emergency condensers for future boiling water reactors. These loops with a complex two-phase flow and phase change in the presence of non-condensable gases need to be well understood in order to guarantee an efficient operation of their design.

1.2 Sump Cooling Concept.

Weishäupl and Bittermann (1993) originally proposed the sump cooling concept of Fig. (1.1) as a safety system for passive decay heat removal from the reactor sump of an advanced light water reactor. After the core melt is spread in the sump, the core melt is flooded from above by the sump water from the IRWST. The water enters the sump area via flooding pipes, which are passively opened due to the radiation heat of the core melt. The subcooled water is heated up by the core melt and starts boiling. A boiling driven mixed convection on short-term and a transition from two-phase to single-phase flow on long-term are expected in the cooling system.

However, this sump cooling concept does not fulfil the licensing requirement of a guaranteed basement integrity in case of an ex-vessel core melt accident. High long-term melt temperatures impose a potential risk for the integrity of the protective layer in the basement and it was recommended to enhance the basement cooling capacity. Therefore an upgraded basement cooling concept for a future light water reactor was designed, which is

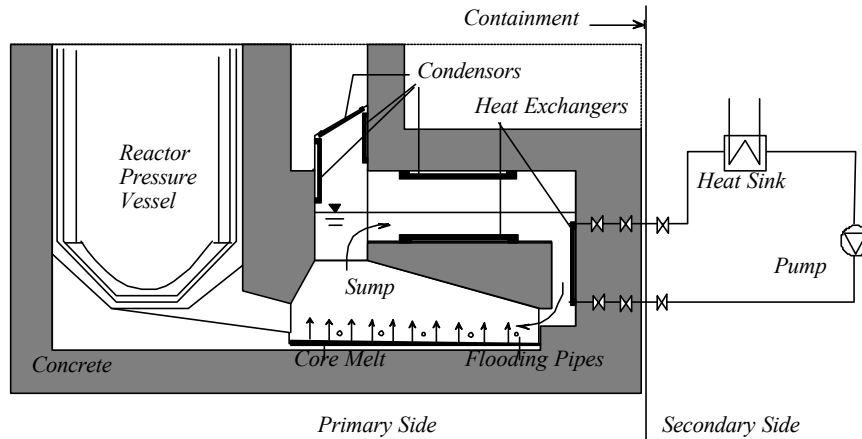


Figure 1.1: First Sump Cooling Concept for an advanced light water reactor.

represented in Fig. (1.2).

For this upgraded basement cooling concept a heat transfer analysis of the horizontal cooling channels in the basement was performed by Schmidt et al. (1999). To guarantee the decay heat removal, the minimal water flow in the cooling channels had to be analysed. The minimal water flow was estimated by envisaging a stable, stationary, stratified two-phase-flow. Thereby the two-phase flow heat transfer calculation was reduced to the single-phase heat transfer calculation of the cooling water. For the void fraction calculation the cases of co-current and counter-current flow were considered following the Chexal-Lellouche model. These strong simplifications give an estimation of the minimal water flow for a single active cooling channel but do not envisage the dynamic behaviour of the total system. Although the two-phase flow pattern and stability are not any more relevant under severe accident conditions, it is however important to prove that a sufficient amount of cooling channels will operate. It is not excluded that the operation of some cooling channels will be affected by flashing effects with local vapour accumulation. An irregular spreading of the core-melt leading to a non-uniform distribution of the heat load for the basement can in stagnant water induce a geyser with local high heat loads during the long incubation period and with

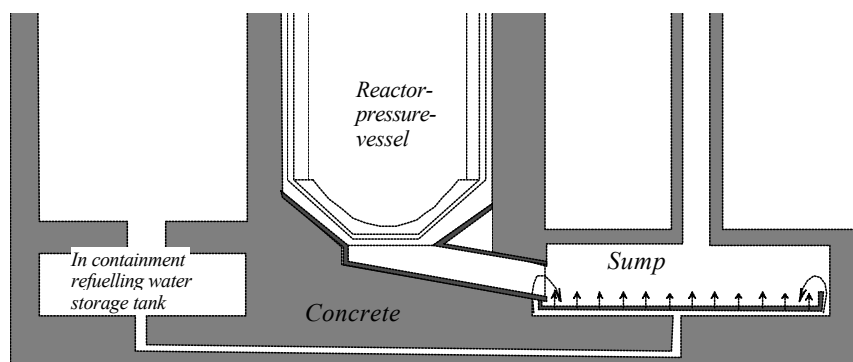


Figure 1.2: Upgraded Basement Cooling Concept for an advanced light water reactor.

local high pressure peaks during the short expulsion period. Probably three-dimensional effects are of significance, so that a different operation of the cooling channels may be expected for different designs of the chimneys collecting the two-phase mixture of several channels.

The upgraded basement cooling concept can be optimised by investigating the grouping of the horizontal channels. Considerable knowledge about the BWR thermal-hydraulic instabilities (of the hydrostatic head driven type or of the density wave driven type) is available in the literature. A global description of the thermal-hydraulic stability is given in terms of the Phase Change Number and Subcooling Number by Zuber (1970, 1976) or by van der Hagen (1997). However only limited research on geyser, the phenomenon that occurs in stagnant water, is performed by Aritomi et al. (1992).

1.3 Objective.

In the safety concept of a future light water reactor the decay heat removal for the ex-vessel core melt down accident has to be analysed from Weishäupl and Bittermann (1993). For licensing purposes it has to be proved that a safety system can remove the decay heat from a flooded core in the sump out of the containment with a sufficiently high heat transfer rate so that the containment integrity remains unaffected. Thereby passive safety systems are envisaged because of their automatic, inherently safe operation, independent of human reliability. Such a passive safety system can be designed based on a boiling induced natural convection cooling loop. Moreover subcooled nucleate boiling offers the potential of removing heat with a high heat transfer rate at low temperature differences. The behaviour of such a cooling loop with subcooled boiling at a heated bottom plate and with flow instabilities such as geysering has been investigated in the test facility SUCOT (Sump COoling Two-phase), constructed at IKET. The test facility scales with the full height of the prototype, so that buoyancy effects and the bubbly flow development of such a cooling loop under fairly reactor-typical conditions can be demonstrated.

The experiments are accompanied by numerical calculations using the CFD code CFX4.1 with additionally implemented and validated models, Janssens-Maenhout (1999).

Chapter 2

Experimental Setup.

2.1 Description.

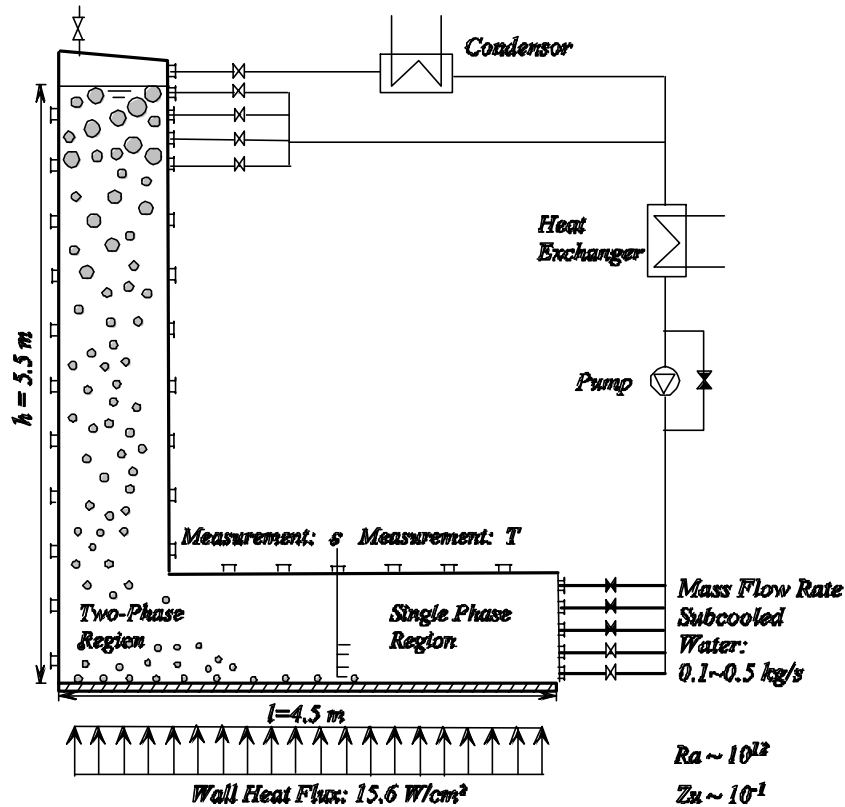


Figure 2.1: Sketch of the test facility SUCOT

In the test facility SUCOT, which is made of an aluminium-glass construction and which consists of a horizontal section with heated bottom plate and a vertical riser section with a hydrostatic head of 0.55 bar , the two-phase flow phenomena have been investigated under atmospheric pressure. The test facility is sketched in figure 2.1 and consists of a L-shaped slab geometry with a length $l = 4.50 \text{ m}$, width $w = 0.94 \text{ m}$, height $h = 5.5 \text{ m}$ and depth

$d = 0.12m$. The width of the horizontal respectively the vertical section are $w_l = 0.9m$ and $w_h = 0.95m$. A first description is given by Janssens-Maenhout (1999) and a more detailed technical description of the test facility has been reported by Daubner, Janssens-Maenhout and Knebel (2001).

Two operation modes, mixed convection and natural circulation, are possible. Here the mixed convection operation mode has been envisaged, in which subcooled water is pumped into the horizontal lower duct and heated up by the hot bottom plate, simulating a core melt. The crust of the core melt can be smooth or fragmented. The surface type may vary from a smooth heated surface to a heated surface covered by a layer of small particles. In the case of a smooth heated surface, the classical boiling model at the heated bottom plate with onset of vapour generation after a single-phase entrance length can be used, whereas the case of a vaporising gravel bed can be modelled as an isothermal boundary layer with a constant vapour source term. Here the case of a heated surface has been described with an appropriate boiling model. The bubbles generated at the heated boundary, are transferred to the bulk fluid. In the bulk the bubbles are dragged with the saturated fluid flow, establishing a disperse two-phase region. If the bubbles are not condensed in a subcooled region, they reach the chimney, where they can rise up and continue to grow in size.

2.2 Equipment and Instrumentation.

The bottom plate of the horizontal section is heated up by 7 *Cu*-blocks, in which 4 electrical heaters of $10kW$ electrical power are embedded. A maximum total wall heat flux of $150kW/m^2$ can be reached. The heat leaks thereby amount up to $5 \sim 6 kW$. The heat losses are mainly caused by heat conduction over the large surface area of the flow sections, although all glass windows of the flow section are isolated. The heat losses have been estimated from the heat balance with the enthalpy difference measured between inlet and outlet of the flow test sections under single phase flow condition.

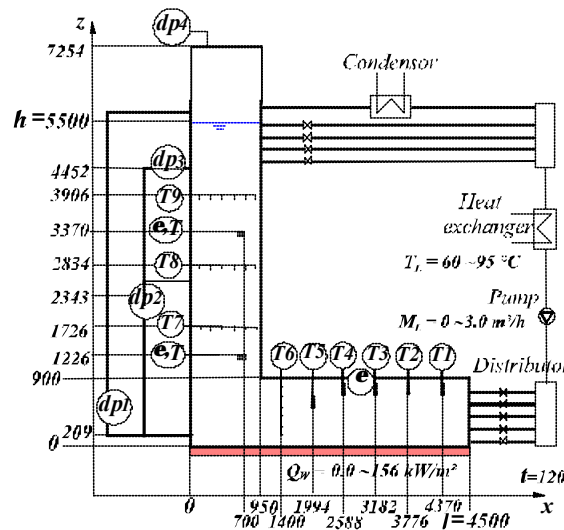


Figure 2.2: Position of the instrumentation in the test facility SUCOT.

Equation	Effect	Single-Phase	Two-Phase
Momentum	Friction	$Re = \frac{u_{Lin} w}{\nu_L}$	$N_D = \frac{U_{Gj Out}}{u_{Lin}} = \frac{\langle 1 - \varepsilon_{Out} \rangle (u_G - u_L)}{u_{Lin}}$
	Buoyance	$Ra = \frac{\beta g \Delta T_{Sub} h^3}{\lambda_L \nu_L / \rho_L c_{pL}}$	$N_{Fr} = \frac{\Delta \rho u_{Lin}^2}{\rho_G g h \langle \varepsilon_{Out} \rangle}$
Temperature	Heat transport	$Pe = \frac{\rho_L c_{pL} u_{Lin} w}{\lambda_L}$	$N_{Sub} = \frac{\Delta \rho c_{pL} \Delta T_{Sub}}{\rho_G \Delta h_{LG}} = \frac{\Delta \rho \Delta h_{Sub}}{\rho_G \Delta h_{LG}}$
	Heated Wall	$Bi = \frac{\dot{Q}_W w}{\lambda_{LWall} \Delta T_{Sub}}$	$N_{PCh} = \frac{\Delta \rho \dot{Q}_W}{\rho_G \dot{M}_L \Delta h_{LG}} = \frac{\Delta \rho \Gamma_G / w}{\rho_G \rho_L u_{Lin} / l}$
Geometry	Two-dimensional	$N_l = \frac{l/w}{h/w}$	$N_l = \frac{l/w}{h/w}$

Table 2.1: Dimensionless Numbers for single- and two-phase mixed convection.

In the horizontal lower duct 6×18 $Ni - CrNi$ -thermocouples of type K for temperature measurements and a gamma densitometer with a ^{137}Cs source for void measurements have been installed. The measurement techniques are described in Knebel and Janssens-Maenhout (1998). In the horizontal lower duct temperature profiles have been measured by the 5×18 traversable thermocouples of type K (indicated as $T1, T2, T3, T4$ and $T5$ in Fig. 2.2) and 1×6 fixed thermocouples of type K (indicated as $T6$ in Fig. 2.2). During the transient experiment the traversable thermocouples have been fixed at the position given in Fig.2. In the vertical riser 3 differential pressure cells measure respectively the pressure drop over the total riser ($dp1$ in Fig. 2.2), the pressure drop over the first half section of the riser with $\Delta z = 2343 - 209mm$ (indicated as $dp2$) and the pressure drop over the second half section of the riser with $\Delta z = 4452 - 2343mm$ ($dp3$ in Fig. 2.2). At the top of the riser the gauge pressure in the vapor space is recorded (indicated as $dp4$ in Fig. 2.2). Additionally, 3×6 thermocouples (in Fig. 2.2) indicated as $T7, T8$ and $T9$ and 2×4 thermocouples with 2 fibre optical probes are inserted in the riser.

2.3 Scaling.

The test facility SUCOT can be scaled by the height h and the width w regarding the geometry, by the mass flow rate $\dot{M}_{Lin} = \rho_L u_{Lin} h d$ and the subcooling $\Delta T_{Sub} = T_{Sat} - T_{Lin}$ regarding the inlet conditions, by the wall heat source $\dot{Q}_W = \dot{q}_W l d$ regarding the boundary condition, and by the water properties $\rho_L, \nu_L, \beta, \lambda_L, c_{pL}, \Delta h_{LG}, T_{Sat}, \rho_G$ regarding the fluid. In table 2.1 the different dimensionless numbers, dedicated to a partially single-phase flow and a partially disperse two-phase flow are listed. The dimensionless numbers for single-phase flow region point out some analogy with those of the two-phase flow region, so that in the limit of a two-phase flow region with vanishing void fraction, the two-phase flow dimensionless numbers continuously turn over to the single-phase dimensionless numbers. The single-phase mixed convection flow is typically described by the Reynolds Number Re , the Rayleigh Number Ra , the Péclet Number Pe and the Biot Number Bi . The behaviour

Table 2.2: Range of experimental conditions for SUCOT.

Exp. cond.	Set points
Hor. length	4.5 m
Inlet temp.	50 ~ 100°C
Inlet vol. rate	0 ~ 0.8 kg/s
Wall heat flux	0 ~ 150 kW/m ²
Initial level	2.0 ~ 5.5 m

Dimensionless n°	Order of Magnitude
Rayleigh N°	$Ra = \beta_L g \Delta T_{Sub} w_h^3 / (\kappa_L \nu_L) \sim 1.E11$
Prandtl N°	$Pr = \nu_L / \kappa_L \sim 7.E0$
Aspect Ratio	$N_R = w_h / h \sim 2.E - 1$
Phase change N°	$N_{PCh} = \Delta \rho Q_W / (\rho_G M_L \Delta h_{LG}) \sim 1.E1 \sim 1.E2$
Subcooling N°	$N_{Sub} = \Delta \rho c_p \Delta T_{LSub} / (\rho_G \Delta h_{LG}) \sim 1.E1 \sim 1.E2$

of the two-phase flow can from Ishii and Zuber (1970) be characterised by the Subcooling Number N_{Sub} , representing the ratio of the inlet subcooling to the latent heat, and by the Phase Change Number N_{PCh} , describing the ratio of the inlet mass flux to the evaporation mass flux. The N_{PCh} and N_{Sub} dimensionless numbers are coupled over the mixture quality at the outlet $x_{eqOut} = \frac{\Delta h_{Out} - \Delta h_{Sub}}{\Delta h_{LG}}$ by the relationship $N_{PCh} - N_{Sub} = x_{eqOut} \frac{\Delta \rho}{\rho_G}$, so that for identical N_{PCh} and N_{Sub} a similar quality development of the flow is preserved. Since the quality and the void fraction are coupled over the relationship $\frac{x_{eq}}{1-x_{eq}} = \frac{\rho_G u_G \varepsilon}{\rho_L u_L (1-\varepsilon)}$ the ratio of the drift to the inlet velocity, defined as Drift Number N_D , has to be considered in order to preserve also the void fraction distribution, Zeller (1992). In case of mixed convection the dimensionless Froude Number N_{Fr} is additionally needed from Van Bragt and Van der Hagen (1998), indicating the ratio of the inertia to the gravity force. Finally, the two-dimensionality can be taken into account by the geometric ratio N_i .

2.4 Experimental Conditions.

The working fluid is water and the range of the experimental conditions is listed in table 2.2. The experimental conditions, depending on the wall heat flux Q_W , liquid mass flow rate M_L and subcooling ΔT_{Sub} are specified by the Phase change number N_{PCh} and the Subcooling number N_{Sub} as derived by Ishii and Zuber (1970) from the drift-flux model, considering the three mixture conservation equations. The more detailed two-fluid model with 6 equations still suffers from incomplete closure relationships, modelling phase interactions. Moreover scaling with 1 common time scale is not any more possible with the two-fluid model. The definition of the Phase Change and Subcooling number have been extended in order to be also applicable for the case of zero inlet mass flux. The definitions used are

$$N_{PCh} = \frac{Q_W / (\rho_G \Delta h_{LG})}{M_L / (\rho_L - \rho_G)} \quad \text{and} \quad N_{Sub} = \frac{\rho_L - \rho_G}{\rho_G} \frac{c_p (T_{Sat}(p_{in}) - T_{Sat}(p_{out}))}{h_{LG}}. \quad (2.1)$$

The Phase change number represents the ratio of the evaporation reaction time constant and the fluid residence time constant whereas the Subcooling number represents the enthalpy

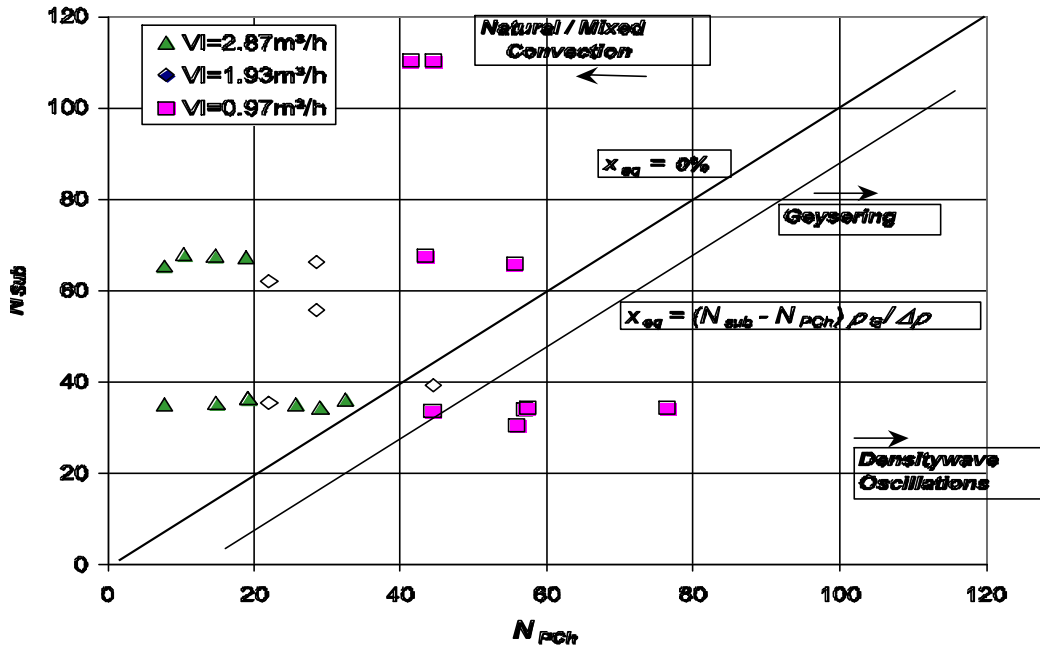


Figure 2.3: Operational stability diagram.

difference of the saturated fluid at the outlet to the saturated liquid at the inlet, scaled with the latent heat. The relationship between N_{PCh} and N_{Sub} is still given by the quality x_{eq} of the mixture in thermodynamic equilibrium. Additionally to N_{PCh} and N_{Sub} the classical single-phase flow dimensionless numbers are given in table 2.2.

An overview of all working points or tests with non-zero inlet mass flow rate is given in the operational diagram of N_{Sub} versus N_{PCh} in Fig. 3. This operational diagram represents at one side the single-phase flow regime and at the other side the geysering regime. Using the extended definition 2.1 the working points with zero mass flux can be situated on the line of zero mixture quality.

2.5 Operating Range and Stability Limits.

An overview of all working points, which were set in different tests, is given in the operational diagram of N_{Sub} versus N_{PCh} in figure 2.3. This operational diagram represents which mixture quality was reached in the test facility and therefore correlates with the two-phase flow pattern. As the transition from one flow pattern to another induces instabilities from Yadigaroglu (1981), the diagram especially indicates the stable and the unstable flow regimes. During the operation of the test facility regimes with quiescent subcooled boiling as well as regimes of geysering are observed. In a first step, reported in chapter 3 the stable regimes are envisaged, for which a bubbly flow with small void fraction, generated by nucleate boiling, establishes in the chimney. These are the stable initial conditions for the second step. During this second step, reported in chapter 4 the unstable two-phase flow phenomena with flashing, and in particular geysering, are investigated.

Chapter 3

Numerical Simulation.

3.1 Model Assumptions and Equations.

For the numerical simulation of such dispersed two-phase flow systems the Eulerian two-fluid-model is widely used. Thereby the two phases are described separately by two interpenetrating fields and coupled by closure relationships for interphase exchange of mass, momentum and energy.

Ensemble-averaging $\langle \rangle_k$ of the local, momentaneous conservation equation of mass, momentum and energy for each phase k yields from Lahey (1995) with density ρ_k , velocity \mathbf{u}_k and enthalpy h_k under pressure p the following mass, momentum and energy equations of the two-fluid-model:

$$\frac{\partial (\varepsilon_k \rho_k)}{\partial t} + \nabla \cdot (\varepsilon_k \rho_k \langle \mathbf{u}_k \rangle_k) = \langle m_{ik}''' \rangle_k + \Gamma_k \quad . \quad (3.1)$$

$$\begin{aligned} & \frac{\partial (\varepsilon_k \rho_k \langle \mathbf{u}_k \rangle_k)}{\partial t} + \nabla \cdot (\varepsilon_k \rho_k \langle \mathbf{u}_k \rangle_k \langle \mathbf{u}_k \rangle_k) + \varepsilon_k \nabla p \\ = & \varepsilon_k \rho_k \underline{\mathbf{g}} + \nabla \cdot \varepsilon_k \left(\langle \underline{\underline{\boldsymbol{\tau}}_k} \rangle_k - \langle \underline{\underline{\boldsymbol{\tau}}_k}^{\mathbf{Re}} \rangle_k \right) + \langle m_{ik} \mathbf{u}_{ik} \rangle_k + \sum_j \mathbf{Z}_{jk} \quad . \end{aligned} \quad (3.2)$$

$$\begin{aligned} & \frac{\partial (\varepsilon_k \rho_k \langle h_k \rangle_k)}{\partial t} + \nabla \cdot (\varepsilon_k \rho_k \langle \mathbf{u}_k \rangle_k \langle h_k \rangle_k) - \varepsilon_k \frac{\partial p}{\partial t} - \nabla \cdot \varepsilon_k p \langle \mathbf{u}_k \rangle_k - \varepsilon_k \langle q_k''' \rangle_k \\ = & \nabla \cdot \varepsilon_k \left(\langle \underline{\underline{\mathbf{q}}_k}'' \rangle_k - \langle \underline{\underline{\mathbf{q}}_k}''^{\mathbf{Re}} \rangle_k \right) + \varepsilon_k \langle \underline{\underline{\boldsymbol{\tau}}_k} - p_k \underline{\underline{\mathbf{I}}} \rangle_k \cdot \nabla \cdot \langle \mathbf{u}_k \rangle_k + \langle m_{ik} h_{ik} \rangle_k + q_{ik}''' \quad . \end{aligned} \quad (3.3)$$

The interphase mass exchange is modelled in equation 3.1 by a decreasing bubble size for condensation in the bulk region $\langle m_{ik}''' \rangle_k$ and by a growing and detaching bubble for vapour generation at the heated wall Γ_k . In the momentum equation 3.2 the interfacial forces are represented by $\sum_j \mathbf{Z}_{jk}$ and $\langle m_{ik} \mathbf{u}_{ik} \rangle_k$ represents the momentum exchange due to phase change. The interphase heat exchange in equation 3.3 is described by the volumetric heat released during reaction q_{ik}''' between both phases and by the enthalpy exchange due to phase change $\langle m_{ik} h_{ik} \rangle_k$. The turbulent fluctuations of velocity and enthalpy field are

taken into account by the Reynolds' stress tensor and turbulent heat flux. The closure relationships has to be additionally conceived, so that the behaviour of the disperse flow can be reflected in the numerical simulation. For the extended derivation of the closure relationships is referred to Janssens-Maenhout (1999). To cope fully with the observed non stationary strong change in bubbly flow behaviour in the SUCOT test facility, the evolution of the interphase exchange has to be taken into account by an additional transport equation for the interfacial area density from Ishii, Wu, Assad and Uhle (1998). Then a numerical tool will be available for reliable simulations of such passive safety cooling systems with dispersed two-phase flow.

3.2 Boundary Conditions and Initial Flow.

As boundary conditions an inlet mass flux and an outlet pressure boundary are set. The walls are treated adiabatically, except the bottom plate. Here two kinds of boundary conditions may be posed. For the case with the smooth heated surface, a heated wall with given heat flux as boundary condition. As long as the point of onset of vapour generation has not been reached, a buoyant single-phase flow establishes. After the point of onset of vapour generation a boiling model for the interfacial phase change must be applied with appropriate characteristics for the surface roughness, the heat transfer coefficient and nucleation site density. In case the bottom plate is covered with a gravel bed, the phase change at the heated boundary with given temperature can be modelled as an isothermal vapour source term. In order to reduce the computational time in a first effort the setup is confined to a simplified steady state and two-dimensional flow case.

For the heated single-phase flow the diffusive and convective heat transport, enhanced by the buoyance effect result in the temperature and velocity profile of Figs. 3.1 and 3.2 over the whole test facility for the case $T_{Lin} = 333K$, $\mathbf{u}_{Lin} = 0.2m/s$. The buoyant flow with unstable stratification in this geometry with huge dimensions of length and height costs a long CPU-time, since the characteristic time constant for the heat diffusion in the computational flow area $\tau_{DS} = \rho_L c_p L^2 / \lambda_L$ takes $7 \cdot 10^7 s$.

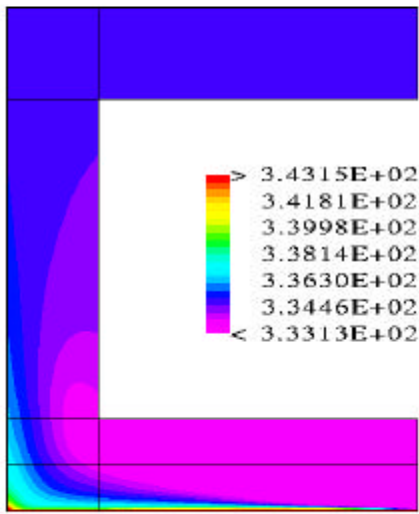


Fig. 3.1: T_L in vertical mid plane

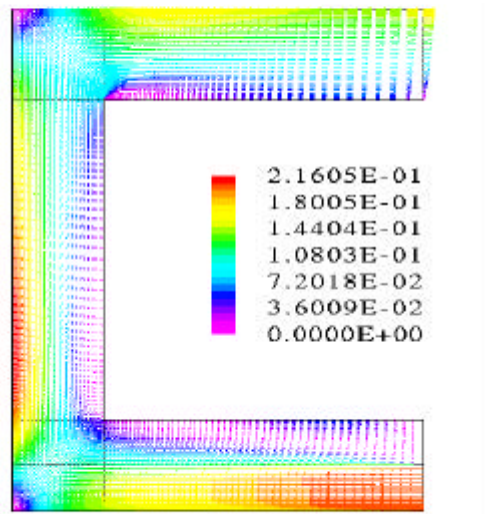


Fig. 3.2: \mathbf{u}_L in vertical mid plane

To validate the numerical simulation the temperature profiles, measured in the horizontal duct along a vertical rack at the positions with a flow entrance length of $0.130m$, $0.724m$, $1.318m$ and $3.100m$ have been successfully compared with the calculated ones in Fig. 3.3. The calculated thermal boundary layer and the almost isothermal heated up pool above do agree with the measurements. The different mixing up of the colder flow and the heated pool may be due to the lack of some turbulence effects in the modelling. The temperatures at the boundaries are in the measurements somewhat lower because of some heat losses in despite of the isolation.

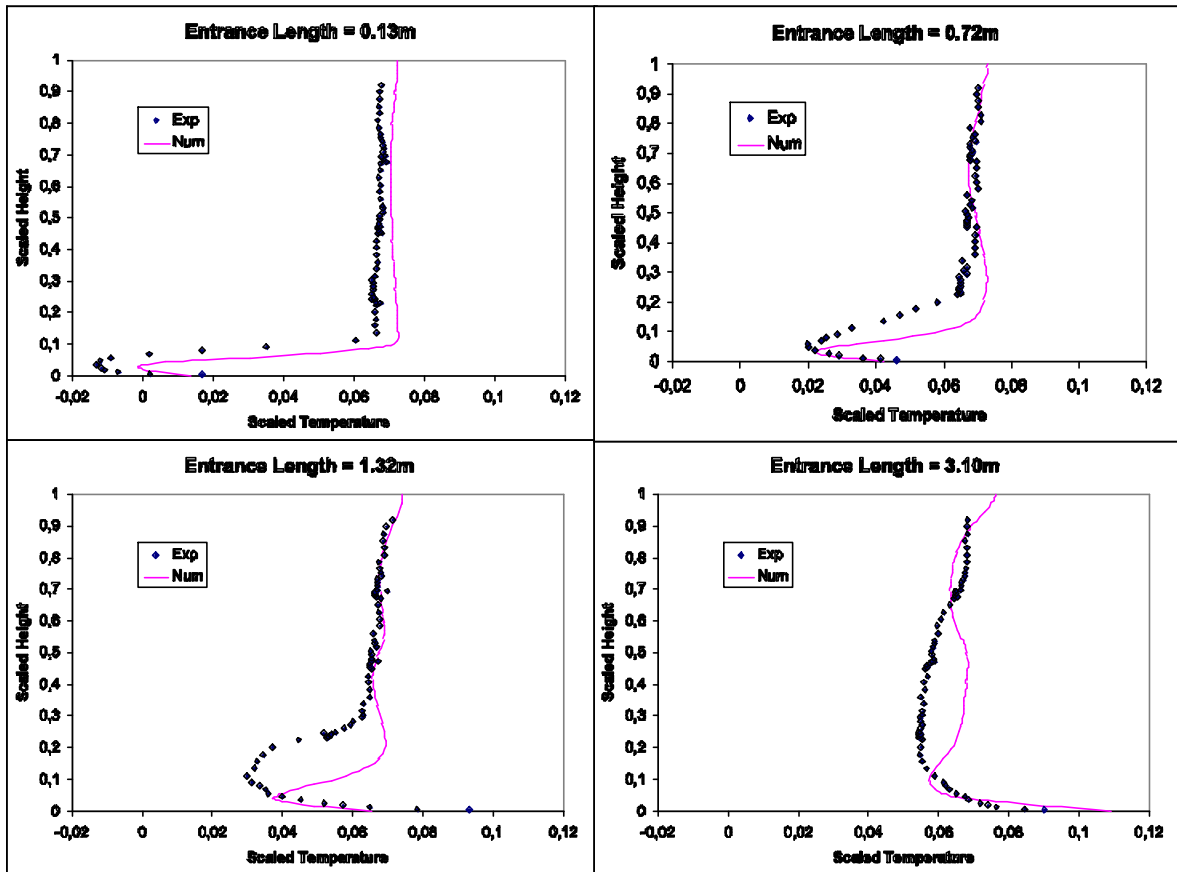


Fig. 3.3: Typical temperature profiles along vertical axes in the horizontal duct

3.3 Subcooled Boiling in the Horizontal Duct.

A further extension by modelling subcooled boiling with a vapour source term at the heated wall and with a condensation source term in the subcooled bulk has been performed. The model of the vapour source term Γ_G at the heated wall is valid for water-vapour systems under pressures $p_L < 1 \cdot 10^6 Pa$ and heat fluxes $< 1 \cdot 10^6 W/m^2$, so a maximum void of 0.3 is generated. The model here is based on the approach of Lahey and Moody (1979) and Kurul (1990).

If $T_L \geq T_{Sat}(p_L)$ a vapour source is under the mechanistic approach from Yadigaroglu and Bensalem (1987) composed of the active nucleation site density N_{as} , the bubble detachment frequency f and the bubble diameter D_A , each depending on the wall heat flux or the wall

temperature.

$$\Gamma_G = N_{as}(T_W) \cdot \rho_G \frac{\pi}{6} (D_A(T_W))^3 \cdot f \left(\left| \underline{\mathbf{q}}''_{\mathbf{w}} \right| \right) \quad . \quad (3.4)$$

3.3.1 Bubble Formation.

The active nucleation site density depends on the wall roughness (especially the mouth diameter and opening angle β_m) and is based on experimental data from Whang and Dhir (1993) given as a function of the critical bubble diameter $D_C = \frac{4\sigma T_{Sat}}{\rho_G \Delta h_{LG}(T_W - T_{Sat})}$ and of the given wetting angle φ :

$$N_{as}(\beta_m < 90^\circ, 18^\circ \leq \varphi \leq 90^\circ) = 5 \cdot 10^{-27} (m^4) \cdot \frac{(1 - \cos \varphi)}{D_C^6} \quad . \quad (3.5)$$

3.3.2 Bubble Detachment.

The bubble detachment diameter D_A is determined by the Correlation of Cole and Rohsenow (1969) as function of the modified Jakob Number $Ja^* = \rho_L c_{pL} T_{Sat} / \rho_G \Delta h_{LG}$ and the Laplace-length $\Lambda = (\sigma / g \Delta \rho)^{\frac{1}{2}}$:

$$D_A = 1.5 \cdot 10^{-4} \cdot \Lambda \cdot Ja^{* \quad 5/4} \quad . \quad (3.6)$$

From Malenkov (1973) the detachment frequency f is derived of the perturbation velocity in the fluid reflux after bubble detachment $f \cdot \pi D_A$, composed of the thermodynamic evaporation rate and the fluid dynamic waves driven by buoyance and capillarity:

$$f \cdot \pi D_A = \frac{\left| \underline{\mathbf{q}}''_{\mathbf{w}} \right|}{\rho_G \Delta h_{LG}} + \left(\frac{D_A \left| \underline{\mathbf{g}} \right| (\rho_L - \rho_G)}{2(\rho_L + \rho_G)} + \frac{2\sigma}{D_A(\rho_L + \rho_G)} \right)^{\frac{1}{2}} \quad . \quad (3.7)$$

3.3.3 Heat Balance at the Wall.

The heat transfer has been modelled by three different correlations. One takes into account the heat transfer to the fluid in the single phase region $\left| \underline{\mathbf{q}}''_{\mathbf{w1}} \right|$, the remaining wall heat flux is then split up in a part for the evaporation $\left| \underline{\mathbf{q}}''_{\mathbf{w2}} \right| = \Gamma_G \Delta h_{LG}$ and a part to heat up the reflux of the cold bulk water after a bubble detachment $\left| \underline{\mathbf{q}}''_{\mathbf{w3}} \right| = \left| \underline{\mathbf{q}}''_{\mathbf{w}} \right| - \left| \underline{\mathbf{q}}''_{\mathbf{w1}} \right| - \left| \underline{\mathbf{q}}''_{\mathbf{w2}} \right|$. There are for $\left| \underline{\mathbf{q}}''_{\mathbf{w1}} \right|$ a single phase heat transfer correlation and for $\left| \underline{\mathbf{q}}''_{\mathbf{w3}} \right|$ the experimental correlation of Del Valle and Kenning (1985) applied.

3.3.4 Condensation in the Subcooled Bulk.

Following the vapour bubble model of Wolfert, Burwell and Enix (1978) the condensation source term is determined by the conductive-convective interfacial heat transfer. The heat

transport from the vapour to the surrounding water is described by the heat transfer coefficient α_{Bi} of Ranz and Marshall (1952):

$$\alpha_{Bi} = \frac{2\lambda_L}{D_B} + \frac{0.6\lambda_L}{D_B} Re_B^{\frac{1}{2}} Pr_L^{\frac{1}{3}} \quad . \quad (3.8)$$

Under the assumption of saturation state inside the bubble, the heat losses of the vapour correspond to mass losses regarding the energy balance of the vapour bubble. This mass loss or decrease in bubble size is coupled to a change in volume fraction:

$$\langle m'''_{iG} \rangle_G = \frac{6\varepsilon_G}{\pi D_B^2} \cdot \frac{\pi \lambda_L}{\Delta h_{LG}} \left(2 + 0.6 Re_B^{\frac{1}{2}} Pr_L^{\frac{1}{3}} \right) \cdot (T_{Sat} - T_L) \quad . \quad (3.9)$$

The boiling model is validated by simulating the void generation and transition from single-phase to two-phase flow in an internally heated annular water flow with subcooled nucleate boiling measured by Bibeau and Salcudean (1994). Here the Figs. 3.4 and 3.5 represent qualitatively the void and velocity profiles over the whole test facility for the case of a fully opened inlet with $\mathbf{u}_{Lin} = 0.2m/s$. The temperature has been kept saturated and a constant vapour source term without condensation has been modelled.

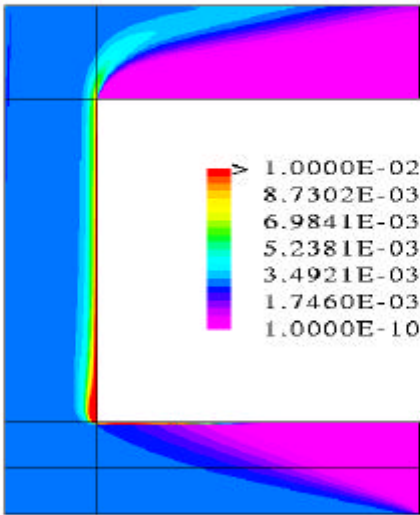


Fig. 3.4: ε_G in vertical mid plane

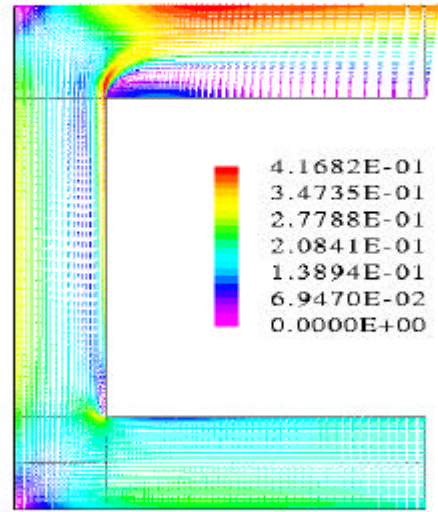


Fig. 3.5: \mathbf{u}_L in vertical mid plane

3.4 Bubbly Flow in the Chimney.

Under the assumption of an ideal dilute bubbly flow, with bubbles as non-interacting, small spherical and non-deformed particles, physical models for the interfacial forces have been derived from the forces on a particle volume, induced by the surrounding fluid under Lagrangian approach. The interfacial forces have been determined by the following closure relationship from Anglart, Nylund, Kurul and Podowski (1993):

$$\begin{aligned} \sum_j \mathbf{z}_{jL} = & -C_D 6\varepsilon_G \rho_L / D_B |\langle \mathbf{u}_G \rangle_G - \langle \mathbf{u}_L \rangle_L| (\langle \mathbf{u}_G \rangle_G - \langle \mathbf{u}_L \rangle_L) - C_{TD} \rho_L \langle k_L \rangle_L \nabla \varepsilon_G \\ & - C_L \rho_L \varepsilon_G (\langle \mathbf{u}_G \rangle_G - \langle \mathbf{u}_L \rangle_L) \times \langle \nabla \times \mathbf{u}_L \rangle_L - 0.5 \rho_L \varepsilon_G (\langle D_t \mathbf{u}_G \rangle_G - \langle D_t \mathbf{u}_L \rangle_L) \end{aligned} \quad (3.10)$$

The first term represents the drag force modelled with the drag coefficient C_D as a function of the Reynolds number Re_B . The dependence of the Eötvös number has been neglected. The second term is the turbulent diffusion force, with a turbulent diffusion coefficient varying as $C_{TD} = 0.01$ to 0.1 for a disperse bubbly flow. Due to turbulent fluctuations of the fluid velocity field, void peaks are attenuated. The third term is the lift force, acting on bubbles which are unequally surrounded by the fluid flow and modelled by a lift coefficient varying as $C_L = 0.1$ to 0.5 . The derivation is valid for high Re , for viscous shear flow another expression of Saffman may be preferred. In shear layers this force induces void peaking. The last term represents the virtual mass, a force appearing when the relative velocity changes. The changes in the kinetic energy of the fluid around the bubble can be interpreted as an additional mass of the bubble to accelerate. Near the wall the lift force is not capable to prohibit the bubble of penetrating the wall. This effect is often modelled by an additional wall lubrication force, but here undertaken by additional boundary condition for the void at the wall.

The models of the interfacial forces are validated by simulating the void redistribution in a turbulent bubbly flow experiment from ? with different local air injections. Here a qualitative picture of the effect of the interfacial forces in the chimney with a hydrostatic head of $2m$ water column and upwards directed inlet velocities $\mathbf{u}_{Lin} = 0.02m/s$ and $\mathbf{u}_{Gin} = 0.2m/s$ has been given in Figs. 3.6 and 3.7. The volume fraction distribution results from the imposed pressure over the column. Although for the case of small bubbles ($D_B = 2mm$) a smooth intension of wall peaking in the beginning may be recognised, globally a central peaking void distribution, as clearly seen for the case of larger bubbles ($D_B = 5mm$) may be expected in the chimney. This has also been observed for tubes of such larger diameter by Hills, Cheng and Azzopardi (1998). However in case of geysering with sudden evaporation, the adiabatic wall sides may form nucleation sites generating vapour bubbles.

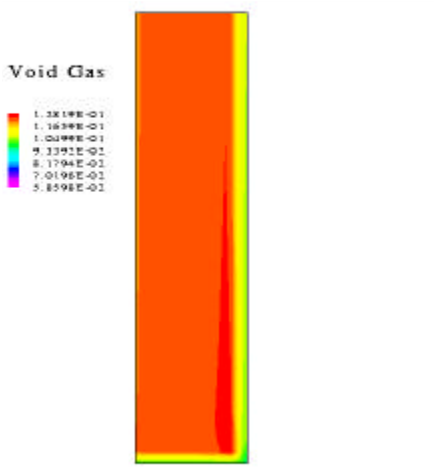


Fig. 3.6: $\varepsilon_G(w/2)$ for $D_B = 2mm$

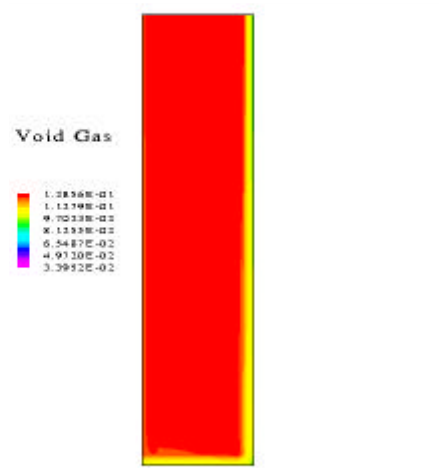


Fig. 3.7: $\varepsilon_G(w/2)$ for $D_B = 5mm$

3.5 Concluding Numerical Results.

The numerical investigation concentrated on the modelling of a dispersed two-phase flow under the assumption of an ideal, dilute bubbly flow. A numerical tool is developed, which is able to deal with both, single-phase and two-phase flow with small void simultaneously. This guarantees a continuous transition from a single-phase flow to a two-phase flow. The two-phase flow is described by means of the two-fluid model. Over the whole computational area an ensemble-averaged continuous field for each phase is available. In addition to the single-phase liquid flow a disperse gas flow as second field with the properties of small spherical bubbles is overlaid. The two interpenetrating fields are coupled with each other by mass, momentum and heat exchange terms, which have been modelled separately.

In the vertical chimney an isothermal bubbly flow is modelled with a momentum exchange term. The model for the interfacial momentum exchange is derived from the resulting force of a single bubble in a liquid flow with consideration of a drag, lift, virtual mass and turbulent dispersion.

In the horizontal duct a non-isothermal bubbly flow with heat and mass transfer is described. The model for the interfacial heat exchange is derived from an empirical heat transfer correlation of Nusselt for a bubble in a liquid flow. The vapour in the bubble is assumed to be saturated, with a saturation temperature corresponding to the pressure in the bubble. The heat exchange between the vapour and the surrounding liquid induces a bubble shrinkage and so a mass exchange. The mass transfer results for superheated regions in a vapour source term and for subcooled regions in a condensate source.

The small-scale, thermodynamic phenomena of fully developed nucleate boiling at a heated wall have been additionally modelled by integral correlations. In superheated regions the vapour source and the wall temperature are iteratively derived. The vapour source is constituted by the active nucleation site density, the bubble detachment diameter and the bubble detachment frequency. These parameters derived by empirical correlations as a function of the wall temperature. The wall temperature is determined by a coincidence of three heat transfer mechanisms. single phase heat transfer, an adiabatic transfer of latent heat for bubble formation and an enhanced heat transfer at the water backflow after detachment. The validity range of the boiling model at the wall is restricted to wall heat fluxes, generating a maximal void of 0.3. The validity range is chosen opposite to other multiphase-multicomponent codes in this way, that subcooled boiling at moderate wall heat fluxes under atmospheric pressure can be modelled.

The models developed and implemented in the code CFX4.1 are validated by Janssens-Maenhout (1999) and provide a numerical tool for the simulation of mixed convection with boiling and condensation phenomena, as met in the test facility SUCOT. Experiments in SUCOT indicate, that the flow pattern differs from an ideal dilute bubbly flow. Bubbles of different form and size are observed. An extension of the validity range of the models for non-ideal bubbly flows with different bubble classes of different sizes is desirable. At the present stage, the numerical tool developed can be applied for a first design optimisation of the sump cooling concept.

Chapter 4

Geysering Experiments.

4.1 Description of the Phenomena.

Depending on the causing mechanism, negative resistance, time-delayed feedback or thermal nonequilibrium, flashing or boiling flow instabilities have been classified by Ozawa (1999) respectively into the three categories: (1) the Ledinegg instabilities with related pressure drop oscillations, (2) the density wave oscillations and (3) the geysering. In the early seventies the nuclear industry analyzed flow instabilities in Boiling Water Reactors (BWR) and investigated the first two categories, especially the second one. For a one-dimensional description of flashing Ishii and Zuber (1970) set up a general dimensionless drift-flux model, which is still used. The criterium for instability was given as function of the Phase change number N_{PCh} and the Subcooling number N_{Sub} .

A first classification was given by Boure, Bergles and Tong (1973). The flashing types concerned mainly forced circulation and density wave oscillation with high steam quality for the BWR conditions, whereas geysering was only mentioned. Density wave oscillations have been experimentally investigated by Yadigaroglu and Bergles (1972) in large detail. Fukuda and Kobori (1978) made a subtle classification of various types density wave oscillations. Lahey and Yadigaroglu (1982) examined the relationship between Ledinegg and density wave stability criteria. They showed that to determine whether a system is stable regarding excursive instabilities, one only needs to examine the zero frequency limit of the linear model used for the analysis of density wave oscillations.

This paper focuses on the third category of geysering, here defined as repeated vaporization, caused by thermal nonequilibrium due to a change in hydrostatic head. Experimental studies in a natural circulation system are limited and mainly performed by Griffith (1962), Ozawa, Nakanishi, Ishigai and Tarui (1979) and Aritomi, Chiang and Mori (1993). Already Griffith reported geysering with periods of the order of 10 to 100 seconds, which disappears under pressurized conditions. Geysering has only clearly been defined by Ozawa, Nakanishi, Ishigai, Mizuta and Tarui (1979) as nonlinear oscillation due to the liquid superheat and self-evaporation. Ozawa noticed additionally to Griffith's findings a stabilizing effect of the inlet velocity and destabilizing effects of the riser length and the heat flux. Based on the experimental results he established a one-dimensional model, representing the principal mechanism of geysering. Later on Aritomi et al. (1993) investigated the instability by using two communicating fluid columns and explained one-dimensional geysering by a transition

from bubbly flow to slug flow.

More recently Jiang, Yao, Bo and Wu (1995) pointed out that the nucleation location for the geysering and the flashing are different. In the case of geysering the self-evaporation is initiated at the bottom heated section, whereas in the case of flashing the evaporation wave starts at the top and moves then downwards. According to our definition the flashing defined by Jiang can be interpreted as geysering. Van der Hagen, Stekelenburg and Van Bragt (1997) stated that geysering occurs in stagnant heated liquid and is dominated by gravity effects in the riser. He uses the model of Ishii but introduces a modified Subcooling number with the saturation temperature at the outlet pressure.

The flashing has been mainly investigated in small, vertical tubes with a heated section and a riser section. Under the low mass flux conditions and with a free liquid surface at the outlet the flashing becomes mainly buoyance driven and can be classified as geysering. Up to now only one-dimensional models are available in literature. However, to describe the flow behavior in real geothermal power sites or cryogenic pipelines one-dimensional models are not satisfying.

Here an experimental study on geysering in two dimensions is performed. A similar principle mechanism as in the case of one-dimensional geysering is observed. The heated fluid is transported to regions at smaller hydrostatic head with lower saturation temperature and becomes superheated. When void is generated, the hydrostatic head and the corresponding saturation temperature are reduced and the self-evaporation is reinforced. However since the flow cross-section of the riser allows a two-dimensional flow behavior, the geysering does not occupy the whole cross-section. Moreover turbulent convective rolls strongly affect the extension of the vapor plume during the self-evaporation.

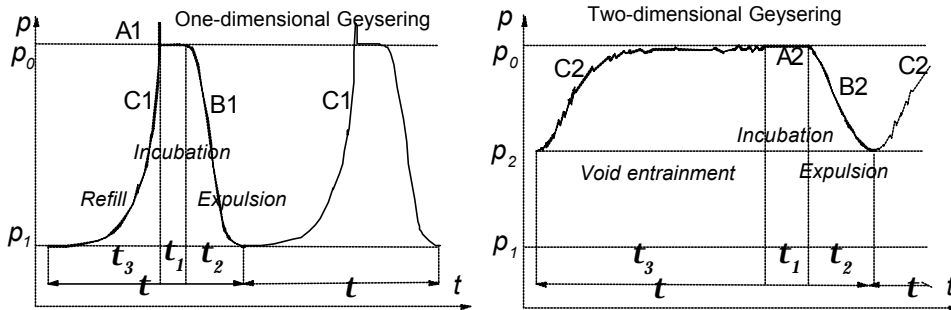


Figure 4.1: Comparison between one-dimensional and two-dimensional geysering.

A division of one geysering period into three phases, analogously as in Ozawa's findings could be performed. After an incubation phase an onset of steam formation is initiated, which then expands sidely and upwards during the expulsion phase and finally ends up with a void entrainment phase. The first phase A of incubation is similar as the incubation phase in the one-dimensional geysering. The second phase B of expulsion differs in strength. In comparison to the one-dimensional geysering case the expulsion phase in the two-dimensional case is shorter and accompanied by smaller pressure movements. Therefore the pressure recovery in the third phase C shows a completely different character as the refill phase in the one-dimensional geysering case. The third phase of a geysering period in

a two-dimensional channel is identified as void entrainment phase. A fast pressure recovery with a strong mixing and entrainment of void by the turbulent convective rolls is observed. Fig. 4.1 shows the typical differential pressure signal during geysering with the different pressure recoveries C1 and C2 for the one-dimensional respectively two-dimensional case.

4.2 Instability Properties of the Test Facility.

In the test facility, described under section 2.1, the geysering due to a depressurization from maximum 1.55 bar to 1 bar has been investigated. The test facility is appropriate to investigate geysering because of its height. Moreover due to the large flow cross-section of the vertical section, two-dimensional effects on the geysering could be clearly observed. The shape of the test facility SUCOT ("SUmmp COoling Two-phase") has originally been conceived to investigate sump cooling by a passive two-phase loop in the safety concept of a future light water reactor, as explained in chapter 1. The L-shape did not disturb the measurements of the geysering phenomenon in the vertical section. The geysering was always initiated in the vertical channel and never reached the horizontal section. Low heat fluxes at the bottom boundary and low mass fluxes, including zero mass flux at the inlet are envisaged, as shown in Fig. 4.2.

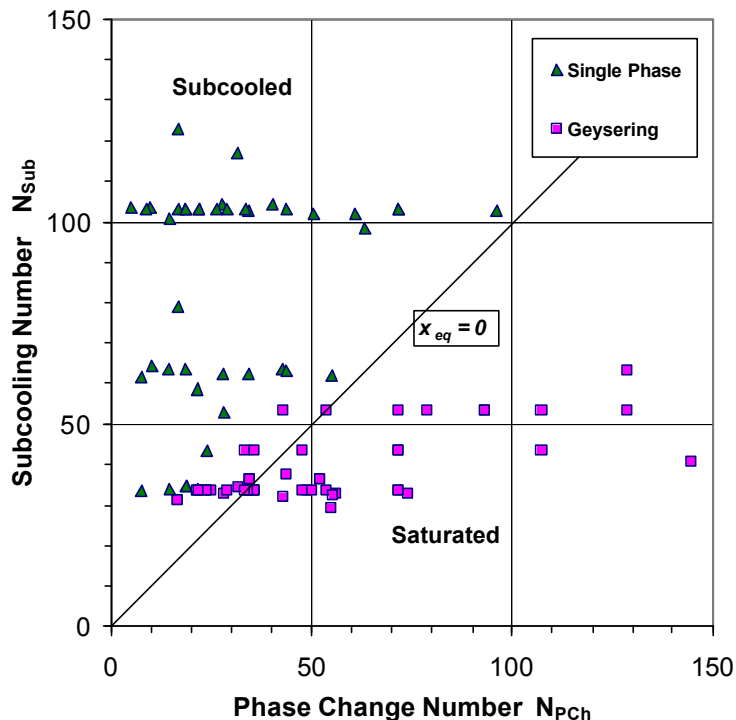


Figure 4.2: Operational diagram for geysering experiments.

The transient flashing behavior has been observed by the differential pressure and temperature measurements recorded with a measuring data rate of 1 Hz during the measurement time of 1 h at different positions in the vertical and horizontal flow sections.

4.3 Characteristic Pressure Behaviour.

In the profile of dp_1 the three phases of incubation, expulsion and void entrainment can be clearly recognized. The total pressure drop dp_1 is mainly affected by the void entrainment and recirculation in the vertical flow section, and is therefore not mostly appropriate to count the geysering periods. The structure of the recirculation is proven by the signal dp_3 since flow accelerations cause an underpressure for downward flow respectively an overpressure for upward flow. The pressure drop dp_2 shows that the geysering never reaches the bottom part of the vertical section and never propagates into the horizontal section.

The profile of the gauge pressure dp_4 in the vapor room above the outlet free surface shows up the highest movements. Therefore this signal is used for determining the periodicity of the geysering. The signal dp_4 indicates clearly the vaporization during the geysering and therefore measures the geysering frequency. The integrated value of the condensing water at the outlet over $1h$ agrees well the integral pressure movement of dp_4 .

The temperature profiles indicated a gradually decrease of temperature with increasing height. The profiles $T7$, $T8$, and $T9$ in the middle of the riser show a strong mixing of the two-phase flow. Because of the short measurement time of fibre optical probes the void measurements did not represent the periodicity of the void behavior during geysering in SUCOT. The void measurements just confirmed the variety in size and form of some clusters of bubbles.

4.4 Characteristic Profile of the Geysering Strength.

4.4.1 Geysering Strength as Function of the Wall Heat Flux.

The cumulative time distribution of the pressure signal dp_4 in the vapor room at the outlet allowed filtering of the pressure peaks due to geysering out of the noise in the boiling two-phase mixture. Thereby the geysering strength $S_{Geysing}$ has been defined as

$$S_{Geysing} = \frac{1}{N_p} \sum (dp_4 - dp_{threshold}) . \quad (4.1)$$

The geysering strength $S_{Geysing}$ has been analyzed as function of the energy input $Q_{Geysing}$ for the geysering. Fig. 4.3 shows $S_{Geysing}$ as function of $Q_{Geysing}$ for different inlet mass fluxes. After exceeding a minimum heat input the geysering strength $S_{Geysing}$ starts to increase strongly with increasing geysering energy $Q_{Geysing}$, especially in the case of low mass flux but then tends to increase more smoothly. From Fig. 4.3 a threshold for a geysering of non-zero strength can be derived.

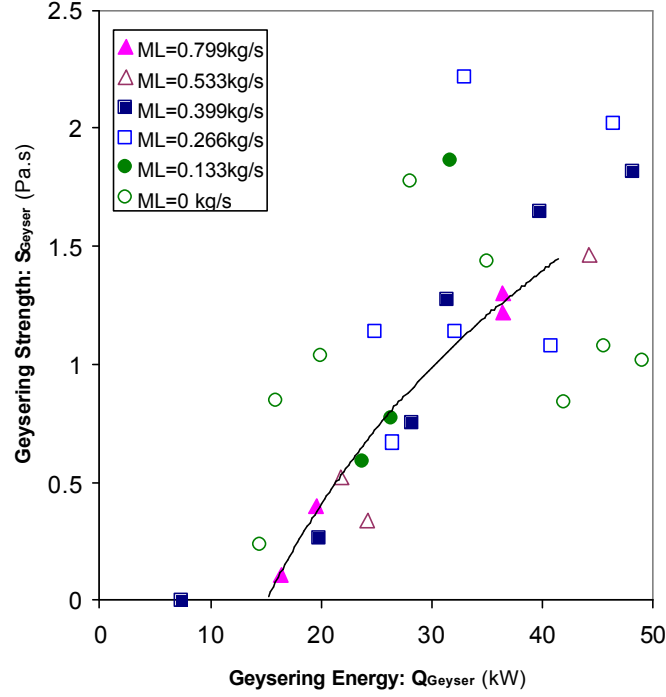


Figure 4.3: Geysering strength over energy.

4.5 Characteristic Profile of the Geysering Frequency.

4.5.1 Geysering Frequency as Function of the Wall Heat Flux

The geysering frequency $f_{Geysing}$ is determined by the number of pressure peaks N_p during the measuring time τ_p of 1h:

$$f_{Geysing} = \frac{N_p}{\tau_p} . \quad (4.2)$$

The frequency of the geysering has been derived applying a discrimination procedure with an exceed of $2mbar$ onto the pressure signal of dp_4 . The qualitative result of the geysering frequency is not affected by the chosen exceed value. This discrimination procedure has been used because the Fourier Transform of the pressure signal did not result in a spectrum indicating a specific frequency for the case of low heat flux. The frequency $f_{Geysing}$ has been analyzed as function of the heat input $Q_{Geysing}$ for the geysering, defined as

$$Q_{Geysing} = \dot{Q}_W - \dot{M}_L c_{pL} (102^\circ C - T_{Lin}(^\circ C)) . \quad (4.3)$$

In the calculation of the geysering energy $Q_{Geysing}$ the value of $102^\circ C$ for the temperature at the onset of steam formation has been chosen because with this value the highest correlation factor of the temperature measurements was obtained. The experimental results of $f_{Geysing}$ as function of $Q_{Geysing}$ for all the experiments with the different inlet parameters are represented in Fig. 4.4. Once a minimum heat input is exceeded, the geysering frequency

f_{Geyser} enhances proportionally with increased geysering energy Q_{Geyser} . This minimum heat input is needed to cover the heat losses. This result characterises the two-dimensional geysering phenomenon. In the one-dimensional case Ozawa, Nakanishi, Ishigai, Mizuta and Tarui (1979) observed a decrease of the geysering frequency with increased geysering energy. The well correlated data in Fig. 4.4 also illustrate the reproducibility of the experimental results.

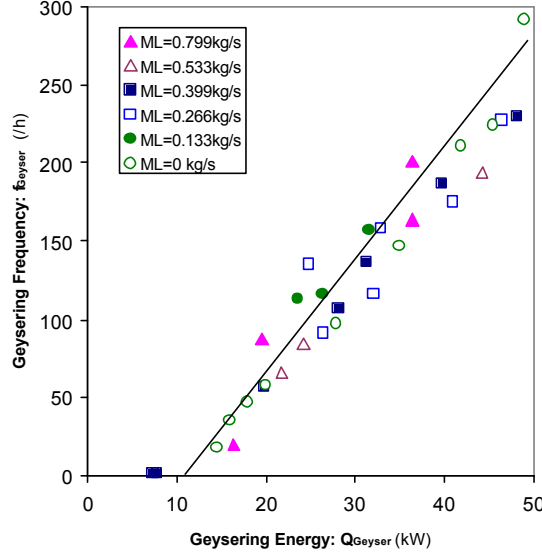


Figure 4.4: Pressure peaks over energy

4.5.2 Geysering Frequency as Function of the Initial Hydrostatic Head.

Additionally experiments at zero mass flux have been performed for different initial hydrostatic heads, changing the original water level z_0 from $5.5m$ in steps of $0.5m$ towards $2.5m$. At lower water level boiling at the heated bottom plate occurs at lower temperature. The geysering frequency f_{Geyser} enhances with decreased water level z as shown in Fig. 4.5. Due to the change in the volume of the vapor space, a scaled step of $2mbar \cdot (z_0 - z)/z_0$ instead of the constant $2mbar$ step was applied in the discrimination procedure for the signal dp_4 . Additional influence of the condenser ability has been neglected. Scaling of the geysering energy Q_{Geyser} with the enthalpy of the total volume of saturated water in the riser, defined as

$$Q_{Geyser} = \frac{Q_{Geyser}}{\rho_L w_h z d \Delta h_{LG}} \quad (4.4)$$

yields a unique correlation between f_{Geyser} and Q_{Geyser} . This is represented in Fig. 4.6 and means that the total energy stored in the geysering, scaled with the initial water volume is for a given heat input constant. This confirms that the geysering in the vertical section is not disturbed by the horizontal section of the test facility.

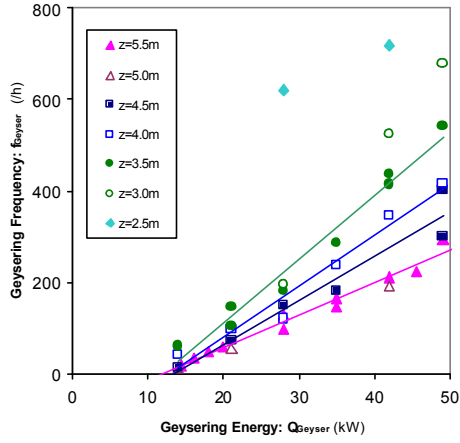


Fig.4.5: Different initial waterlevels

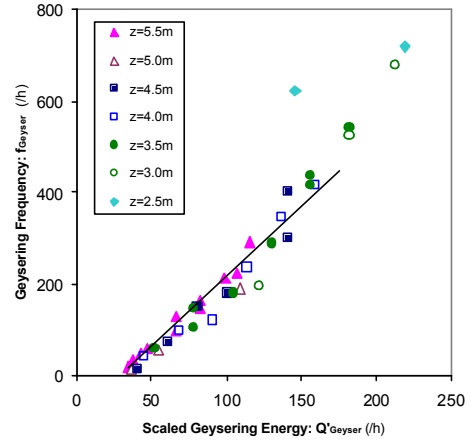


Fig.4.6: Frequency / scaled energy

The general behavior that the geysering frequency decreases with increased initial water level z is related to the enlarged water volume of the riser. By increasing the water level the aspect ratio N_R is reduced and the vertical section resembles the one-dimensional channels with geysering at lower frequency. The temperature profiles of the thermocouples in the riser only depend on the distance between the thermocouples and the water level.

Below $3.0m$ the strong increase in geysering frequency indicates a transition to another instability mode of the geysering. Moreover the temperature signals in the horizontal and vertical section for the cases of $3.0m$ to $5.5m$ water level differ completely from the temperatures recorded in the case of $2.5m$ water level. The more regular temperature behavior in the case of $2.5m$ water level is strongly influenced by the boiling noise of the horizontal section whereas the irregular temperature behavior in the other cases are due to the strong mixing in the void entrainment phase.

4.5.3 Geysering Frequency as Function of the Riser Width.

The riser width has been reduced from $950mm$ to $307mm$ by inserting a separation plate from the bottom at $z = 0.0m$ until in the vapor space at $z = 6.0m$. At reduced riser width the onset of geysering moved towards higher energy input for the geysering $Q_{Geysers}$, as represented in Fig. 4.7. The geysering frequency also increases with increasing energy input more rapidly in the case of a narrow riser than in the case of a wide riser since a smaller water volume is present in the riser. The comparison of the case with narrow riser width of $307mm$ and the original case with riser width of $950mm$ is complicated by the difference in heat leaks. The influence of the non-active channel of $643mm$ at a temperature some degrees below the temperature in the active channel of $307mm$ could not be estimated.

Clearly a difference in flow behavior was observed. The convective rolls in the riser are much smaller and confirms the scaling of the diameter of those rolls with the channel width. Moreover less mixing was established. This observation was confirmed by the temperature measurements. The temperature profile in the case of narrow riser shows a much smaller fluctuation in the horizontal layers and much larger vertical temperature gradient over

the different layers than the temperature profile in the case of a wide riser. Only the temperature profile T_8 shows larger fluctuations around a mean temperature value, which is situated more close to the maximum value. It can be assumed that T_8 is after a geysering expulsion affected by a reversal of colder water layers. This means that the geysering in the case of a narrow riser does not expand downwards so low as in the case of a wide riser. Experiments in the narrow riser at different initial hydrostatic head are not representing the same tendency as in the original case of the wide riser. This is shown in Fig. 4.8. The dip in geysering frequency can be explained by a different behavior of the two-phase flow with strong flow oscillations. These flow oscillations are more expressed in the case of a narrow riser, since in the case of a wide riser the large volume of water with larger inertia damps this oscillating effect coming from the horizontal section. These flow oscillations also explain the broader scattering of measured geysering frequency data for the narrow riser case in Fig. 4.8.

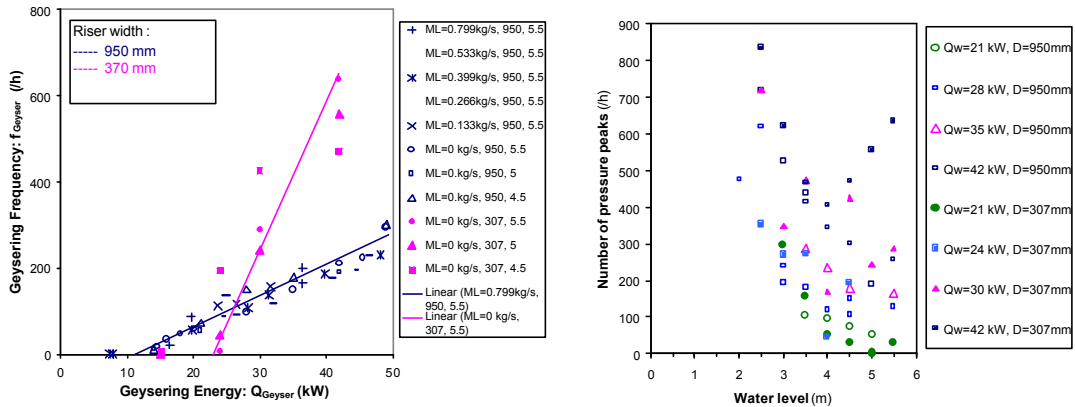


Fig. 4.7: Frequency in a narrow/wide riser. Fig. 4.8: Water width/height dependence.

4.6 Concluding Experimental Results.

Unsteady, subcooled boiling two-phase flow in large two-dimensional geometries are still hard to be numerically simulated and need still experimental, validated correlations. The geysering phenomenon in a two-dimensional flow cross-section is strongly affected by turbulent convective rolls and therefore less violent. One geysering period can be divided in an incubation phase, an expulsion phase and a void entrainment phase.

In the one-dimensional case the geysering frequency decreases by increasing the geysering energy. But in the two-dimensional case the geysering frequency increases by increasing the geysering energy. Moreover by reducing the initial water level the two-dimensional effect becomes stronger and the geysering frequency enhances even more. For high initial hydrostatic head the geysering frequency tends to approach an asymptotic value. The geysering strength enhances also by increasing the geysering energy but tends to approach an asymptotic value for high heat input.

The mixing plays a major role in the geysering phenomena. The onset of geysering can be postponed by inserting separation plates, impeding the establishment of large convective rolls. In a narrow riser the geysering frequency is not reduced proportional with the initial hydrostatic head because of a different flow oscillation behavior.

Chapter 5

Conclusion.

Boiling enables to transfer large amounts of heat at small temperature differences. In particular subcooled boiling is established in many large-scale technical installations, e.g. in power plants for the cooling of surfaces under high heat loads. A technical option in the nuclear industry is the sump cooling concept for future light water reactors. In the case of an ex-vessel core melt accident the sump cooling concept allows the decay heat removal from the core melt, which is spreaded in the sump, by a passive two-phase natural circulation flow. The optimisation and reliability of such a two-phase flow loop with complex interfacial phenomena is experimentally and numerically investigated. Thereby the interfacial heat, mass and momentum exchanges between the two phases have been described. Experiments on the two-phase flow mixed convection have been performed in the test facility SUCOT. Additionally a numerical tool, describing two-phase flow phenomena, with explicit treatment of the interfacial phenomena and subcooled flow boiling has been developed.

The two-phase flow phenomena in the boiling induced mixed convection loop of the test facility SUCOT are described by the dimensionless Phase Change Number N_{PCh} , the Subcooling Number N_{Sub} , the Drift Number N_D , the Froude Number N_{Fr} . The experiments show an unstable dynamic behaviour which is due to the transition from bubbly flow to slug flow. Experimentally a flow pattern map in the (N_{PCh}, N_{Sub}) -diagram indicates in which range the operational parameters are allowed in order to avoid instabilities. For the extrapolation of this stability diagram for other applications, the instabilities of phenomenological origin have to be carefully distinguished from the system dependent instabilities. Here an analytical bifurcation analyses of a simplified one- and two-dimensional boiling induced mixed convection loop would be helpful.

With the two-fluid-model a wide range of two-phase flows in a cooling system can be modelled. Moreover the efficiency of heat transfer for subcooled flow boiling can be estimated and applied for the design of industrial cooling loops. However computational and experimental effort for the modelling of subcooled nucleate boiling is still needed. The simulations with vapour generation need actually a time-dependent analysis of the interfacial area.

Chapter 6

Perspectives

One important perspective of this combined experimental / numerical work, which is in the field of two-phase flow, lies in its possible application to the development of accelerator driven systems (ADS). The main objective on an ADS is its potential to transmute minor actinides and long-lived fission products, thus participating in closing the fuel cycle. Transmutation is an important issue within the Euratom Fifth Framework Programme on Partitioning and Transmutation, European Commission (2001a).

An accelerator driven system consists of three main parts: an accelerator for primary particles (protons), a spallation target in which the protons produce free nucleons (neutrons) in a spallation reaction (external neutron source), and a subcritical blanket in which the fission reaction takes place, producing fission neutrons (internal neutron source) and thermal energy. The protons are injected into the spallation target through a vacuum beam pipe, the beam pipe being closed by a beam window at the end. The spallation target is a heavy liquid metal (e.g. lead Pb or lead bismuth alloy Pb-Bi).

One concept of an ADS, which is investigated in more detail within the "Preliminary Design Study of an eXperimental ADS" Project (PDS-XADS) of the Euratom Fifth Framework Programme (European Commission (2001b)), is the Energy Amplifier Demonstration Facility of ANSALDO, Ansaldo Nucleare (2001). An essential feature of this concept is the natural circulation of the primary coolant within the reactor pool. The natural circulation, which is driven by the density differences between the blanket and the heat exchanger, is enhanced by the injection of the nitrogen cover gas through spargers located in a riser part just above the blanket.

This so-called gas-lift pump system has not been investigated in more detail nor has this gas-lift pump system been numerically/experimentally confirmed.

The knowledge gained within the SUCO Programme, i.e. the modelling of the interfacial forces (Janssens-Maenhout (1999)), the experimental work on flow instabilities in SUCOT of this report, and the modelling of the interfacial area concentration (Janssens-Maenhout and Müller (1999)), can be directly applied to the design of accelerator driven systems. However, the transfer from the two-phase system water / steam to the system lead-bismuth / nitrogen has to be done.

Thus, the results of the POOLTHY Project (Tenchine, Knebel, Jackson and Naviglio (2001)) are of direct relevance to the PDS-XADS Project.

Bibliography

- Anglart, H., Nylund, O., Kurul, N. and Podowski, M. Z.: 1993, CFD prediction of flow and phase distribution in fuel assemblies with spacers, *Proc. of the 1st CFDS Int. User Conf., Oxford, May 6-7, 1993*.
- Ansaldo Nucleare, XADS Pb-Bi Cooled Experimental Accelerator Driven System Reference Configuration Summary Report, ADS1-SIFX 0500 Rev. 0 (2001)
- Aritomi, M., Chiang, J. and Mori, M.: 1993, Fundamental study on thermal-hydraulics during start-up in natural circulation boiling water reactors: II natural circulation oscillation induced by hydrostatic head fluctuation, *J. Nucl. Science and Techn.* **30**(3), 203-211.
- Bibeau, E. and Salcudean, M.: 1994, Subcooled void growth mechanisms and prediction at low pressure and low velocity, *Int. J. Multiphase Flow* **20**(5), 837-863.
- Boure, J., Bergles, A. and Tong, S.: 1973, Review of two-phase flow instability, *Nucl. Eng. Design* **25**, 165-192.
- Cole, R. and Rohsenow, W.: 1969, Correlations of bubble diameters for boiling of saturated liquids, *Chem. Eng. Prog.* **65**, 211-213.
- Daubner, M., Janssens-Maenhout, G. and Knebel, J.: 2002, Technische Beschreibung der Testanlage SUCOT zur Untersuchung einer Wasser/Wasserdampf Zweiphasenströmung, Technical Report FZKA 6683, Forschungszentrum Karlsruhe.
- Del Valle, V. H. M. and Kenning, D. B. R.: 1985, Subcooled flow boiling at high heat flux, *Int. J. of Heat and Mass Transfer* **28**(10), 1907-1920.
- European Commission: 2001, Partitioning and Transmutation: Towards an easing of the nuclear waste management problem, EURATOM Report EUR 19785.
- European Commission: 2001, European research area and proposed direction of EURATOM research in FP (2002-2006), http://europa.eu.int/comm/research/index_en.html.
- Fukuda, K. and Kobori, T.: 1978, Two-phase flow instability in parallel channels, *Proc. 6th Int. Heat Transfer Conf.* **FB**(17).
- Griffith, P.: 1962, ASME paper 62-HT-39, *J. Am. Soc. Mech. Eng.* **62-HT**(39), 1.
- Hills, J., Cheng, H. and Azzopardi, B.: 1998, Void fraction waves in vertical gas-liquid flow in a 150 mm tube, *Proc. of 3rd Int. Conf. on Multiphase Flow, Lyon* pp. 1-8.
- Ishii, M., Wu, Q., Assad, A. and Uhle, J.: 1998, Interfacial area transport equation for two-fluid model formulation, *Proc. of IMuST Meeting, Santa Barbara*.
- Ishii, M. and Zuber, N.: 1970, Thermally induced flow instabilities in two-phase mixtures, *Proc. of 4th Int. Heat Transfer Conf., Paris* pp. B-5.11.
- Janssens-Maenhout, G.: 1999, *Beiträge zur Modellierung und numerischen Simulation von Zweiphasenströmungen mit Wärmeübertragung*, PhD thesis, University of Karlsruhe, FZKA-Report 6228.
- Janssens-Maenhout, G., Daubner, M., Knebel, J. U. and Müller, U.: 1999, Boiling driven mixed convection in a L-shaped slab geometry, *Proc. EURO THERM 63* pp. 189-198.

- Janssens-Maenhout, G., Müller, U.: 1999, A stepwise approach for disperse two-phase flow modelling in cooling Loops, Paper C1 of the 37th European Two-Phase Flow Group Meeting, London, Sept. 28-30, 1999.
- Jiang, S., Yao, M., Bo, J. and Wu, S.: 1995, Experimental simulation study on start-up of the 5MW nuclear heating reactor, *Nucl. Eng. and Design* **158**, 11-123.
- Knebel, J. U. and Janssens-Maenhout, G.: 1998, Boiling induced mixed convection in cooling loops, Proc. of 36th European Two-Phase Flow Group Meeting, Portoroz, June 1-5, 1998.
- Kurul, N.: 1990, *Multidimensional effects in two-phase flow including phase change*, PhD thesis, Rensselaer Polytechnic Institute.
- Lahey, J. R. T.: 1995, The CFD analysis of multidimensional phenomena in multiphase flow, *Proc of 2nd Int. Conf. on Multiphase Flow, Kyoto*.
- Lahey, J. R. T. and Moody, F. J.: 1979, *The Thermal Hydraulics of a Boiling Water Nuclear Reactor*, American Nuclear Society, La Grange Park, Illinois.
- Lahey, J. R. T. and Yadigaroglu, G.: 1982, On the relationship between Ledinegg and density wave instability analysis, *Trans. ANS* **41**, 689-691.
- Malenkov, I. G.: 1973, Detachment frequency as a function of size for vapor bubbles, *Translated from Inzhenerno-Fizicheskii Zhurnal (at the Academy of Sciences of the USSR)* **20**(6), 988-994.
- Ozawa, M.: 1999, Flow instability problems, *Steam Power Engineering: Thermal and Hydraulic Design Principles*. **Chapter 5**, 323-385.
- Ozwaw, M., Nakanishi, S., Ishigai, S. M. Y. and Tarui, H.: 1979, Flow instabilities in boiling channels, part 1: Pressure drop oscillations, *Bull Jap. Soc. Mech. Eng.* **22**(170), 1113-1118.
- Ozwaw, M., Nakanishi, S., Ishigai, S. M. Y., Mizuta, Y. and Tarui, H.: 1979, Flow instabilities in boiling channels, part 2: Geysering, *Bull Jap. Soc. Mech. Eng.* **22**(170), 1119-1126
- Ranz, W. E. and Marshall, W. E.: 1952, Experimental correlation for heat transfer between particle and fluid, *Chemical Engineering Prog.* **48**(3), 141
- Samstag, M.: 1996, *Experimentelle Untersuchungen von Transportphänomenen in vertikalen turbulenten Luft-Wasser-Blasenströmungen*, PhD thesis, University of Karlsruhe.
- Tenchine, D., Knebel, J. U., Jackson, D., Naviglio, A.: 2001, Thermalhydraulics of large pools with immersed heat exchangers and natural convection heat transfer (POOLTHY), EU Co-Sponsored Research on Evolutionary Reactor Safety Concepts, Final Summary Reports INNO Cluster Projects, edited by Bermejo, J. M. and Van Goethem, G., European Commission Report EUR 19788 EN, pp. 79-107.
- Van Bragt, D. and Van der Hagen, T.: 1998, Stability of natural circulation boiling water reactors: Part i - description stability model and theoretical analysis in terms of dimensionless groups, *Nuclear Technology* **121**, 40-51.

- Van der Hagen, T., Stekelenburg, A. and Van Bragt, D.: 1997, Reactor experiments on type-I and type-II BWR stability, *Proc. NURETH 8* **1**, 397-400.
- Wang, C. H. and Dhir, V. K.: 1993, Effect of surface wettability on active nucleation site density during pool boiling of water on a vertical surface, *Trans. ASME Journal of Heat Transfer* **115**, 659-669.
- Weisshäupl, H. A. and Bittermann, D.: 1993, Large spreading of core melt for melt retention/stabilization, *Containment of nuclear reactors : Proc. of 5th int. seminar held in conjunction with 12th internat. conf. on structural mechanics in reactor technology, SMIRT, Karlsruhe, Germany, Aug. 23-24, 1993*, pp. 347-355.
- Wolfert, K., Burwell, M. J. and Enix, D.: 1978, Non-equilibrium mass transfer between liquid and vapour phases during depressurization processes in transient two-phase flow, *Proc. of 2nd CSNI Specialists Meeting, Paris* **1**.
- Yadigaroglu, G.: 1981, Two-phase flow instabilities and propagation phenomena, *Thermohydraulics of Two-Phase Systems for Industrial Design and Nuclear Engineering* pp. 353-403.
- Yadigaroglu, G. and Bensalem, S.: 1987, Interfacial mass generation rate modeling in non-equilibrium two-phase flow, *Multiphase Science and Technology* **3**, 85-127.
- Yadigaroglu, G. and Bergles, A.: 1972, Fundamental and higher-mode density wave oscillations in two-phase flow, *Int. J. Heat Transfer, Trans. ASME* **94**, 189-195.
- Zeller, M. U.: 1992, *Scaled model of a natural-circulation heating reactor*, PhD thesis, ETH Zürich.

Acknowledgement

The authors like to thank the scientific guest, students and technicians for their devoted contribution to the construction, operation and evaluation of this large-scale test facility SUCOT. In particular we like to thank Dr. H. Umekawa from Kansai University Japan for his suggestions to improve the instrumentation of SUCOT, coping with the instability phenomena.

The work was partly supported by the European Commission under the POOLTHY Project number FJ4J-CT95-0003 within the Euratom 4th EU Framework Programme.

Chapter 7

Appendix 1: Prototype Conditions.

A1. From nuclear technology:

Reactor Design	
Technical specification	Order of range
reactor power	1450 MWe = 4250 MWth
number of cooling loops	4
reactor inventory	241 17x17 fuel elements (130 t)
fuel	UO ₂ -MOX (U enriched up to 4.9%)
cycle	12-18-22 months
burnup	50.000-60.000 MWd/t

Table 7.1: Reactor technical specifications for an innovative LWR.

Reactor containment design	
Technical specification	Order of range
containment	cylindrical, double walled
inner wall	reinforced concrete
external wall	reinforced concrete
design pressure	7.5 bar abs.
pressure limit	8 bar abs.
temperature	315-445 K

Table 7.2: Reactor safety specifications for an innovative LWR.

A2. From reactor safety analyses:

Sump cooling concept design for a core melt accident	
Parameter	Prototype 1500 MW PWR
Fluid	water
spreading area	160 m ²
water level	5.5 m
decay heat	25 MW
heat flux	15.6 W/cm ²
objective	guarantee the core melt cooling

Table 7.3: Technical specifications for the sump cooling concept of an innovative LWR.

SUCO-Programm.	
Parameter	Test facility SUCOT
Fluid	water
spreading area	0.45 m ²
water level	5.5 m
decay heat	0.07 MW
heat flux	15.6 W/cm ²
objective	investigate the two-phase flow behaviour

Table 7.4: Technical specifications for the sump cooling concept of the test facility SUCOT.

Chapter 8

Appendix 2: List of Symbols

Symbole.

Scalars:

A_i	m^2	Surface of the Interface
A_{wk}	m^2	Interface of Phase k and the wall
c_p	J/kgK	specific heat capacity
C	—	coefficient
d	m	diameter of tube
D_A	m	Bubble detachment diameter
D_B	m	Bubbel diameter
D_C	m	critical bubble diameter
e_k	m^2/s^2	specific internal energy of Phase k
E_k	m^2/s^2	specific total energy of Phase k
E'_k	m^2/s^2	specific total energy fluctuations of Phase k
f	$1/s$	bubble detachment frequency
h	m	Height of channel
h_k	J/kg	specific enthalpy of Phase k with $h = e + p/\rho$
Δh_{LG}	J/kg	Latent heat
Δh_M	J/kg	Enthalpy difference of the mixture
k_L	m^2/s^2	turbulent kinetic energy of Phase k
k_0	J/K	Boltzmann constant = 13.8066 J/K
l	m	Length
m_{ik}	kg/m^2s	Interfacial mass transport for Phase k
N_{as}	$1/m^2$	activ nucleation site density
p	Pa	Pressure
q'''_{ik}	W/m^3	Interfacial heat for Phase k

q_k'''	W/m^3	Heat source for Phase k
Q	J/kg	specific heat
\dot{Q}	W	heating power
t	s	time
T_k	K	Temperature of Phase k
T_W	K	Wall temperature
T_0	K	Initial / Inlet temperature
V	m^3	Volume
\dot{V}_k	m^3/s	Volumetric mass flux of Phase k
x_{eq}	–	Mixture quality in thermodynamic equilibrium
x, y, z	m, m, m	cartesian coordinates
α	W/m^2K	heat transfer coefficient
α_{Bi}	W/m^2K	interfacial heat transfer coefficient of the bubble
β_L	$1/K$	volumetric expansion coefficient of the liquid
$\Delta\tau$	s	time interval
ε_k	m^3/m^3	Void of Phase k
ϵ_L	m^2/s^3	Dissipationrate of the liquid
Γ_G	kg/m^2s	vapour source density at the wall
κ_L	m^2/s	Temperature conductivityof the liquid $\kappa_L = \lambda_L / \rho_L c_{pL}$
λ	W/mK	heat conductivity
Λ	m	Laplace length
ν_k	m^2/s	kinematic viscosity of Phase k
ρ_k	kg/m^3	Density of Phase k
σ	kg/s^2	Surface tension

Vectors and Tensors:

$\underline{\underline{\mathbf{A}}}$	$[\underline{\underline{\mathbf{A}}}]$	Tensor
$\underline{\mathbf{F}}$	$[\underline{\mathbf{F}}]$	Vector
\mathbf{F}'	$[\underline{\mathbf{F}}]$	Fluctuation of $\underline{\mathbf{F}}$
$\langle \underline{\mathbf{F}} \rangle_k$	$[\underline{\mathbf{F}}]$	for Phase k ensemble averaging of $\underline{\mathbf{F}}$
$\underline{\mathbf{g}}$	m/s^2	gravity
$\underline{\mathbf{j}}_k$	m/s	Volumetric Flux of Phase k
q_i''	W/m^2	interfacial heat source for phase transport
$\underline{\mathbf{q}}_k''$	W/m^2	heat flux of Phase k
$\underline{\mathbf{q}}_W''$	W/m^2	Wall heat flux
$\underline{\mathbf{q}}_k^{Re}$	W/m^2	turbulent heat flux of Phase k
$\underline{\mathbf{u}}_i$	m/s	interfacial velocity
$\underline{\mathbf{u}}_{ik}$	m/s	velocity of Phase k at the interface
$\underline{\mathbf{u}}_k$	m/s	velocity of Phase k
$\underline{\mathbf{Z}}_k$	N	Interfacial force
$\underline{\underline{\Sigma}}$	$1/m$	Surface tensor
$\underline{\underline{\tau}}_k^{Re}$	kg/ms^2	Reynolds Tension
$\underline{\underline{\Xi}}$	W/m^2	Energy of the Interface

Subscripts:

A	bubble detachment
B	bubble
h	maximal, horizontal
C	critical, neutral stable state at bubble formation
C_D	resistance coefficient
G	of Gasphase
h	of heating source
i	at Interface
i	Indices $i = 1, 2, 3$
i	internal
k	of Phase k , $k = L, G$
\mathbf{K}	convective
$\langle \rangle_k$	Ensemble-averaging of Phase k
L	of Liquidphase
\mathbf{L}	Conductive
C_L	Lift coefficient
m	mouth diameter of wall pore
M	of the mixture
n	normal
Out	at Outlet
r	in radial direction
Sat	Saturation condition
Sub	subcooled
Sup	superheated
t	tangential
T	total
C_{TD}	turbulent diffusion coefficient
C_{VM}	virtual mass coefficient
W	at the wall
0	at Inlet
∞	at infinity

Superscripts:

Re	Reynolds
*	modified
\cdot	total time derivative

<i>I</i>	turbulent fluctuation
<i>II</i>	pro surface
<i>III</i>	pro volume

Dimensionless Numbers:

ε_G	$\frac{V_G}{V_G+V_L}$	Void
Gr	$\frac{g \beta_T \Delta T l^3}{\nu_L^2}$	Grashof-Number
Ja	$\frac{\rho_L c_{pL} \Delta T_{Sat}}{\rho_G \Delta h_{LG}}$	Jakob-Number
Ja^*	$\frac{\rho_L c_{pL} T_{Sat}}{\rho_G \Delta h_{LG}}$	modified Jakob-Number
N_{Sub}	$\frac{\Delta \rho c_{pL} \Delta T_{Sub}}{\rho_G \Delta h_{LG}}$	Subcooling Number
Pe	$\frac{u_L D_B}{\kappa_L}$	Péclet-Number
Nu	$\frac{\alpha d}{\lambda}$	Nusselt-Number
Nu_B	$\frac{\alpha_{Bi} D_B}{\lambda_L}$	Bubble Nusselt-Number
Pr	$\frac{\nu_L}{\kappa_L}$	Prandtl-Number
Ra	$Gr \cdot Pr$	Rayleigh-Number
Re	$\frac{u_L d}{\nu_L}$	Reynolds-Number
Re_B	$\frac{u_L D_B}{\nu_L}$	Bubbly Reynolds-Number
Sta	$\frac{Nu}{Re \cdot Pr}$	Stanton-Number
We	$\frac{\rho_L u_G^2 D_B}{\sigma}$	Weber-Number
x_{eq}	$\frac{h_M - h_L}{h_G - h_L}$	Mixture Quality
Zu	$\frac{\Delta \rho \Gamma_G}{\rho_L \rho_G u_L}$	Zuber-Number

Operators:

∇	Gradient
$\nabla \cdot$	Divergence
Δ	Laplace-Operator
$\nabla \times$	Rotation
$\frac{\partial}{\partial t}$	partial time derivative
$\frac{D_k}{Dt} = \frac{\partial}{\partial t} + \mathbf{u}_k \cdot \nabla$	total time derivative for Phase k

Abbreviations

CBD	Computational Bubble Dynamics
CDS	Central Differencing Scheme
CFX4.1	Computational Fluid Dynamics Code of AEA Technology, Version 4.1
DNS	Direct Numerical Simulation
DWR	Druckwasserreaktor
GLE	General Langevin Equation (Stochastic Transport Theory)
HDS	Hybrid Differencing Scheme
IB	Incipience of Boiling
IRWST	In Containment Refueling Water Storage Tank
IPSA	Numerical scheme Inter Phase Slip Algorithm to couple the velocity fields of both phases
IPSAC	Numerical Interphase Slip Algorithm, Consistent Version
KE	Kinetic Equation (Boltzmann Gas Theory)
LES	Large Eddy Simulation
LWR	Light Water Reactor
NVG	Net Vapour Generation Point
ONB	Onset of Nucleate Boiling
QUICK	Quadratic Upwind Differencing Scheme
RDB	Reaktordruckbehälter (= RPV Reactor Pressure Vessel)
SIMPLE	Numerical Semi-Implicit Method for Pressure Linked Equations, SIMPLE Revised and SIMPLE Consistent
SIMPLEC	Numerical Semi-Implicit Method for Pressure Linked Equations Consistent version
SUCOT	Test Facility Sump COoling Two-phase
UDS	Upwind Differencing Scheme
n D	n -dimensional